Dye-Sensitized Solar Cells

DOI: 10.1002/anie.201104605

Hierarchically Assembled ZnO Nanocrystallites for High-Efficiency Dye-Sensitized Solar Cells**

Nafiseh Memarian, Isabella Concina, Antonio Braga, Seyed Mohammad Rozati, Alberto Vomiero, and Giorgio Sberveglieri*

Photoelectrochemical cells[1] are promising devices for cheap, environmentally compatible, and large-scale solar energy conversion as an alternative to conventional solid-state semiconductor solar cells. Among excitonic cells,[2] dye-sensitized cells (DSCs)[3] exhibit the highest performance in terms of energy conversion efficiency and long term stability, despite the fact that the efficiency remains below 13% because of the intrinsic limitation in charge transport. The structure of the photoelectrodes is crucial in determining the functional properties of the photoelectrochemical system. In particular, the photoanode consists of a mesoporous wide-band-gap oxide semiconductor film with a high specific surface (typically a thousand times larger than the bulk counterpart).[4–6] To date, the highest photoconversion efficiency (PCE) has been achieved with film consisting of 20 nm TiO_2 nanocrystallites sensitized by different dye molecules (11.1% for N719 dye,[7] over 10% for "black dye",[8] and 11.4% for C101,[9]). In addition to TiO_2, a series of other n-type metal oxide semiconductors can in principle be used in DSCs, such as ZnO, SnO_2, and In_2O_3. Much attention has been recently devoted to ZnO[10] owing to its higher electron mobility and similar electronic band structure with respect to TiO_2. Various strategies have been addressed to enhance PCE in ZnO-based DSCs, which are mainly based on tailoring the geometrical and structural features of ZnO. A possible solution to reduce electron recombination could be the use of one-dimensional nanostructures that are able to provide a direct pathway for the rapid collection of photogenerated electrons.[11,12] However, only low PCE has been achieved to date, mainly because of the reduced internal surface area of the nanostructures. Hybrid structures have also been tested to improve light collection, such as combination of nanoparticles and nanowires (maximum PCE = 4.2%),[13,14] or hierarchical nanowires (maximum PCE = 2.63%).[15] Another strategy to enhance PCE is application of hierarchical photoanodes composed of large aggregates of nanocrystallites, which can act as light scattering centers while maintaining a high specific surface area.[16–19]

The synthetic procedure of photoanode preparation is crucial to improve PCE: an optimized photoanode composed of just ZnO nanoparticles without any geometrical feature for light confinement or enhanced electron transport resulted in the highest value of PCE (6.58%) for a ZnO-based DSC.[20]

Herein we present the fabrication and characterization of hierarchically structured ZnO-based photoanodes in DSCs to enhance the PCE. Our approach addresses specifically the following points: 1) High optical density of the sensitized layer, allowing complete light absorption in the spectral range of the dye; 2) high light scattering of the absorbing layer, enhancing the time spent by light inside the sensitized film and improving light absorption; and 3) inhibition of back electron transfer between the conducting layer at the anode and the electrolyte. The films are prepared by the simple, cheap, and large-area-scalable spray pyrolysis method. The films are composed of polydispersed ZnO aggregates consisting of nanosized crystallites while submicrometer-sized aggregates act as efficient light scattering centers and nanoparticles provide the mesoporous structure and the large specific surface area needed for high dye loading. Additionally, a ZnO compact layer is intentionally formed between the conducting substrate and the layer composed of polydispersed aggregates. Such a layer acts as an efficient blocking layer for electron back reaction between the conducting glass at the anode and the electrolyte,[21] improving the functional properties of the cells. This is the main innovation with respect to the work of Cao and co-workers,[16] leading to unprecedented PCE up to 7.5%, which is larger than ZnO nanoparticles (6.58%),[20] hierarchically structured ZnO without a blocking layer (5.4%),[16,18] and hierarchically arranged ZnO nanowires (2.63%).[15] As a further benefit, our method is extremely fast (no more than 1.5 h for the complete processing of a photoanode, while typically 8 h[16] or 10 to 14 h[10] are required), enabling its technological implementation.

The compact layer in contact with the conducting glass was deposited by a standard spray pyrolysis procedure starting from a methanol/water solution of zinc acetate dihydrate (see the Experimental Section). The main layer of ZnO aggregates (samples 1–4) was obtained from a mixture composed of an ethanolic suspension of ZnO commercial nanoparticles and a methanol/water solution of zinc acetate dihydrate. Annealing in air followed to induce the sintering of the aggregates. Films (15 ± 1) μm thick are considered in this study. A second set of samples (samples 5, 6), used as a

[*] N. Memarian, I. Concina, A. Braga, A. Vomiero, G. Sberveglieri
CNR-IDASC SENSOR Lab and Department of Chemistry and Physics, Brescia University
Via Valotti 9, 25131 Brescia (Italy)
E-mail: alberto.vomiero@ing.unibs.it
N. Memarian, S. M. Rozati
Physics Department, University of Guilan
Rasht (Islamic Republic of Iran)

[**] Dr. Caterina Soldano is acknowledged for fruitful discussions and suggestions during the preparation of the manuscript. Nicola Poli is acknowledged for his technical assistance in the set-up of the spray pyrolysis apparatus. The CARIPLO Foundation under contract 2008.2393 and Oikos srl (Brescia) is acknowledged for partial funding.

benchmark of the effectiveness of the proposed synthetic route to improve cell performances, was also considered. These samples were obtained by spray pyrolysis of commercial nanoparticles dispersed in ethanol without any other precursor.

The fluorine-doped tin oxide (FTO) conducting layer was prepared according to the procedure that was previously described[22] and exhibits the functional properties suitable for solar cells (transparency over 80% in the visible range and sheet resistance below 10 Ω/□).

Figure 1 shows the scanning electron microscopy (SEM) images of ZnO film with the buffer layer, polydispersed aggregates and their size distribution, and a high-resolution image of single aggregates. The highly disordered structure is visible in Figure 1b; each aggregate consists of closely packed nanoparticles, and the broad size distribution of the aggregates ranges between 100 nm and 600 nm (average diameter: (270 ± 85) nm). This ZnO film has a hierarchical structure, which is delivered directly by the synthetic method. The buffer layer shows a compact structure with respect to the top layer, enabling a blocking action of electron recombination.

The buffer layer is optically transparent, as expected for a ZnO compact film, while the film composed of polydispersed ZnO aggregates appears white, thus confirming the effective scattering action of the particles. In particular, Mie theory[23] and Anderson localization of light[24] provide an exhaustive analytical description of light scattering by spherical and elliptical particles. Resonant scattering may occur when the particle size is comparable to the wavelength of the light. This is exactly the condition of ZnO aggregates within the film, and is the reason for the white color of the aggregates.

One additional advantage of the shape of the aggregates is the broad size distribution (see Figure 1c). In fact, polydispersed aggregates are able to successfully form a highly disordered photoanode, as quantitatively analyzed in Figure 1c. Such a structure can result in random multiple scattering of the light traveling through the film by the so-called Levy paths.[25] The effect would lead to light localization owing to formation of traps for optical confinements, enhancing the probability of light absorption. Additionally, aggregates polydispersed in size are believed to induce light scattering in a broad wavelength region.[26]

The ruthenium complex bis(tetrabutylammonium) *cis*-diisothiocyanato-bis(2,2′-bipyridyl-4,4′-dicarboxylato)ruthenium(II), known as N719 dye, has been used to sensitize the ZnO films. The film is immersed in a 0.5 mM ethanol solution of N719 dye for approximately 2 h. This immersion time was chosen to avoid the dissolution of surface zinc atoms and formation of Zn^{2+}/dye complexes, which is believed to be harmful to the charge transport from the dye to the semiconductor.[27–29]

Investigation of dye loading kinetics was carried out to quantify the relative amount of dye with respect to the asymptotic value expected for long-time impregnation. Dye loading is calculated from UV/Vis measurements after complete removal of chemisorbed dye from oxide surface using 0.1M NaOH aqueous solution.[30] As illustrated in Figure 2 for a sample composed of ZnO aggregates annealed at 450°C, pseudo-first-order kinetics is found, with a time constant of about 12.5×10^{-3} min^{-1}. The best-performing cell (sample 1) presents dye loading of about 80% of the asymptotic value.

The photoanode has a high specific surface area, with a calculated dye loading of 1.5×10^{-7} mol cm^{-2} (relative to the geometric electrode area) from UV/Vis measurements after dye removal using calibrated solutions.[30] Such results are in line with similar experimental findings on similar systems, and confirm the effectiveness of the synthetic route in delivering a mesoporous structure with large internal surface area. All of the samples

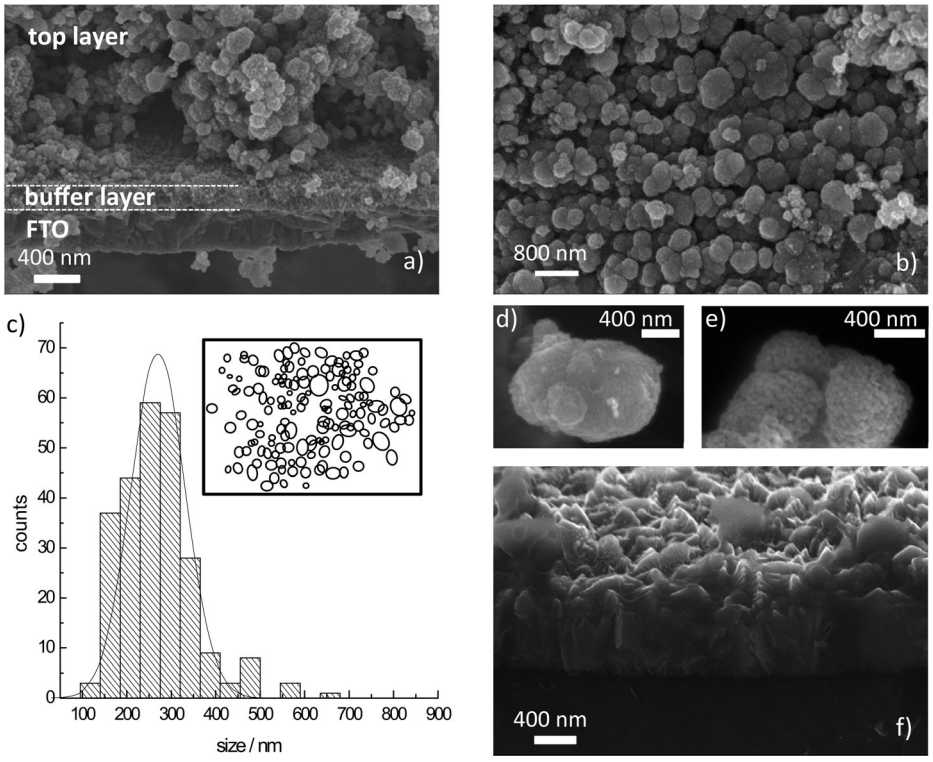

Figure 1. a) Cross-sectional SEM image of the photoanode. The top layer, composed of hierarchically structured ZnO nanocrystals, the compact buffer layer, acting as the blocking element for electron back reaction, and the FTO conducting layer are visible. b) Top view of the absorbing layer, showing a highly disordered structure. c) Size distribution of the aggregates, as estimated by SEM. Inset: Shape analysis of the aggregates from the SEM image in (b), with elliptical shapes predominant. d,e) High-resolution SEM images of two aggregates, showing the closely packed assembly of the nanoparticles. f) High-resolution SEM image of the buffer layer, indicating its compact morphology with respect to the polydispersed aggregates.

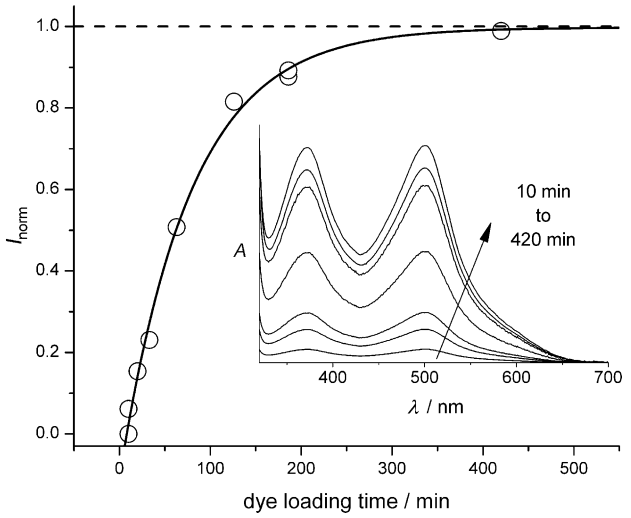

Figure 2. Quantification of dye loading as a function of loading time in ZnO aggregates annealed at 450 °C. The intensity of the absorption band at 500 nm of N719 is monitored as a function of the loading time (10 to 420 min; ○ experimental data, —— exponential fitting). Inset: UV/Vis absorption spectra as a function of different loading times as indicated by the arrow.

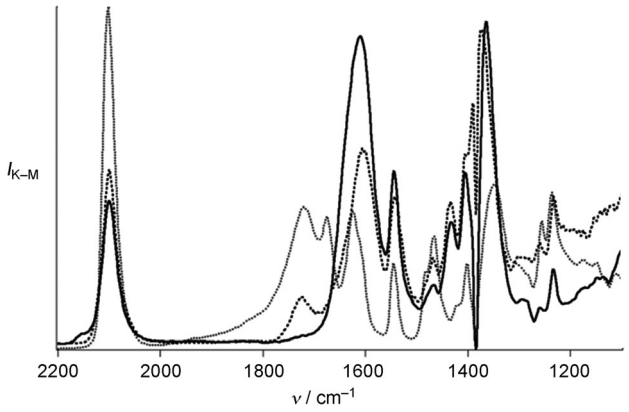

Figure 3. DRIFT spectra of dye N719 (••••), dye N719-sensitized ZnO (——), and dye N719-sensitized TiO_2 (-----).

prepared with ZnO precursors (samples 1–4) have about the same dye uptake ability, so improved functional properties do not rely on enhanced dye loading, but other functional features have to be claimed (such as light management and/or electron transport and collection).

Grafting of N719 dye on ZnO surface has been studied with diffuse-reflectance FTIR (DRIFT) spectroscopy. Figure 3 shows a comparison between the DRIFT spectra of N719 powder, N719-sensitized ZnO, and N719-sensitized TiO_2. The peak owing to the stretching of SCN group is completely preserved in both dye-loaded metal oxide photoanodes, thus indicating that thiocyanate is not involved in binding the metal oxide surface. Stretching of C=O, visible as a double band in the N719 spectrum (1721 and 1675 cm^{-1}), has completely disappeared in the spectrum of loaded dye: ZnO coordinates with all the four carboxylic functions available, as also confirmed by the relevant decrease of the intensity vibration mode of the NBu_4^+ counterion (1466 cm^{-1}). This finding marks a noteworthy difference with respect to dye loading on TiO_2 surface,[31] in which the acidic groups do not bond (stretching C=O at 1726 cm^{-1}). Symmetric O–C–O stretching is visible in the spectrum of loaded ZnO at a higher wavenumbers than the corresponding peak of pure dye (1365 and 1348 cm^{-1}, respectively), while the signal owing to asymmetric O–C–O stretching, although overlapping with the vibration modes of bipyridine rings (centered at 1625 cm^{-1}, shoulder at 1608 cm^{-1}), is much broader and shifted toward lower wavenumbers (1610 cm^{-1}). N719 binds to the metal oxide surface in a chelating/bridging mode,[32] as in the case of TiO_2-loaded photoanodes.

As-prepared ZnO solar cells are characterized by measuring the current–voltage curve while the cells are irradiated by 1.5 G AM simulated sunlight (100 mW cm^{-2}). The transient photovoltage decay[33] is acquired to gain information on electron lifetime as a function of the open-circuit voltage.

In Figure 4 a typical current density (J) versus voltage (V) curves of different ZnO photoanodes are collected. Sample 1, composed of the buffer layer and optimized aggregates, exhibits the best photovoltaic performances in terms of fill factor (FF), short circuit current density (J_{SC}), open circuit voltage (V_{OC}), and photoconversion efficiency (PCE). On the other hand, samples 5 and 6, consisting of only ZnO commercial nanocrystallites, present the lowest J_{SC} and the lowest PCE, owing to poor sintering features, which do not allow creation of a percolating network for electron conduction. Table 1 summarizes the functional parameters of all of the analyzed cells.

Table 1: Preparation details and photovoltaic properties of ZnO photoanodes.[a]

Sample	Annealing temperature	Buffer layer	Load time [h]	V_{OC} [mV]	J_{sc} [mA cm^{-2}]	FF	PCE [%]
1	450 °C	yes	2	640	19.8	0.59	7.5
2	370 °C	yes	2	630	12.8	0.60	4.9
3	450 °C	no	2	650	7.5	0.54	2.6
4	450 °C	no	18	590	7.5	0.49	2.2
5	–	yes	2	630	0.8	0.39	0.2
6	–	no	2	500	0.4	0.50	< 0.1

[a] PCE = photoconversion efficiency, FF = fill factor.

Characteristic electron lifetime (τ_e), obtained by transient photovoltage decay, is given for two selected samples in Figure 4 b to elucidate the influence of the various components of the photoanodes on cell performance. Equation (1),[33] where k_B is the Boltzmann constant, T is the

$$\tau_e = \frac{k_B T}{e}\left(\frac{dV_{oc}}{dt}\right)^{-1} \quad (1)$$

absolute temperature, and e is the elementary charge, gives a fast method to calculate τ_e directly from the transient photovoltage decay. τ_e is intimately related to the nature of the interface oxide/dye/electrolyte.

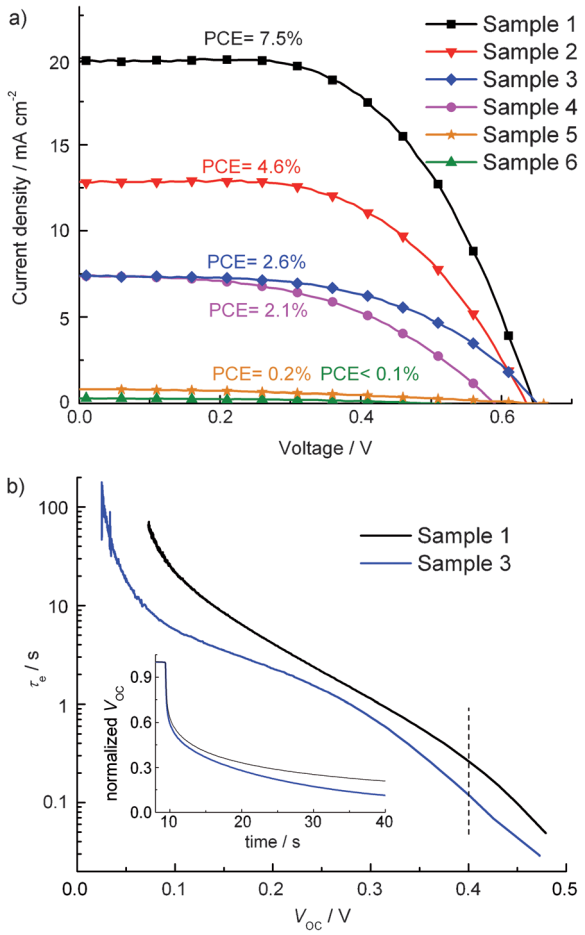

Figure 4. a) *J–V* curves of samples 1–6 under 1.5 G AM simulated sunlight irradiation (100 mW cm^{-2}). b) Electron lifetime versus the open circuit voltage for selected samples. Inset: Transient photovoltage decay.

The current density in a DSC is determined by the initial number of photogenerated carriers, the injection efficiency from dye molecules to semiconductor, and the recombination rate between the injected electrons and oxidized dye or redox species in the electrolyte. It is reasonable to assume the same injection efficiency for the given ZnO/dye/electrolyte system and the same light-harvesting capability for samples 1–4 (as they exhibit similar morphology of the layer composed of ZnO aggregates), so different values of J_{SC} can be ascribed to different mechanisms of charge transport and recombination in photoanodes with different structure.

Specifically, the buffer layer and the firing temperature play a crucial role. The buffer layer relies with inhibition of electron recombination between the TCO at the photoanode and the electrolyte[21] and guarantees enhanced electron harvesting, leading to improved J_{SC}. It is shown experimentally by direct comparison of sample 1 and sample 3, which differ just for the presence of the buffer layer: sample 3 (without a buffer layer) exhibits an electron lifetime that is more than three times lower than sample 1 (with a buffer layer) at 400 mV. Thanks to the presence of the buffer layer, the PCE turns out to be about three times higher (from 2.6% in sample 3 to 7.5% in sample 1). One further proof of the role of the buffer layer is given by the functional properties of samples 5 and 6, which are composed of commercial nanoparticles. Even in these samples, which exhibit poor functional properties, the presence of the buffer layer is able to significantly enhance current density and photoconversion efficiency. Such a positive effect is somehow different with respect to the buffer layer in TiO_2 photoanodes, where limited improvement was observed, which could be attributed to the presence of a compact layer between the FTO and the mesoporous film.[34]

Firing temperature affects the ability of aggregates to form a well-connected network for electron transport: the higher the sintering temperature, the stronger the interaction amongst aggregates. Comparison of sample 1 and sample 2 offers direct evidence of such a mechanism: a higher firing temperature results in a 55% improvement of J_{sc} (from 12.8 mA cm^{-2} to a remarkably high 19.8 mA cm^{-2}), which is reflected in a more than 50% increase in PCE (from 4.9% to 7.5%).

In conclusion, spray pyrolysis has been demonstrated effective for the creation of a nanoengineered DSC photoanode exhibiting optimized optical and electrical features. An unprecedented PCE of 7.5% for ZnO-based DSCs was achieved for a photoelectrode consisting of polydispersed ZnO aggregates of nanocrystallites over a compact ZnO buffer layer and at a firing temperature of 450 °C. Combined optimization of the firing temperature and buffer layer effect is crucial to dramatically enhance the photoconversion efficiency. The process of photoanode preparation is much faster with respect to traditional routes based on the hydrothermal synthesis of ZnO crystallites, thus paving the way for a direct scale-up and industrial exploitation of these results.

Experimental Section

Spray pyrolysis was applied to the formation of a compact buffer layer, a mixed layer of ZnO submicrometer-sized aggregates composed of nanocrystallites, and a layer of commercial nanoparticles. The buffer layer is deposited from ZnO precursor solution (0.24 M, 25 mL methanol/water, 2:1 v/v $Zn(CH_3COO)_2{\cdot}2H_2O$). The mixed layer is formed starting from an ethanolic suspension of commercial nanoparticles (0.5 g in 15 mL ethanol) and of the ZnO precursor solution for spray pyrolysis ($Zn(CH_3COO)_2{\cdot}2H_2O$ 0.55 M, in 40 mL methanol/water, 3:1 v/v). For both the buffer layer and the mixed layer, the carrier gas (N_2) was at pressure of 0.40 bar, the hot plate for sample allocation was at 250 °C, and post-deposition annealing was carried out in the range 350–450 °C for 30 min. Nozzle-to-sample distance: 37 cm for the buffer layer, 25 cm for the mixed layer. A series of samples with and without the buffer layer (samples 1–4) were produced at different annealing temperatures to investigate the effect of the buffer layer and of the annealing temperature on cell performances.

The layers of commercial particles (samples 5, 6) were prepared by spraying the ethanolic dispersion of commercial ZnO nanoparticles. The substrate was kept at 200 °C, the carrier gas pressure was 0.40 bar, and the nozzle-to-substrate distance was 15 cm. This procedure resulted in a powder-like film with quite poor adhesion.

Fluorine-doped tin oxide (FTO) thin film was deposited on glass substrate according to Ref. [22]. A solution of $SnCl_2{\cdot}2H_2O$ in methanol (0.2 M, 40 mL) and NH_4F used as dopant (25 atom%) was used as the starting solution. FTO films with a transparency of more

than 80% and a sheet resistance lower than 10 Ω/□ were used as the electrode.

The oxide photoanodes were dye-sensitized by impregnation into a 5.0×10^{-4} M ethanolic solution of commercial ruthenium-based molecule dye N719 (Solaronix). The best sensitization time (2 h) was chosen on the basis of literature results. After impregnation samples were carefully washed with ethanol to remove unadsorbed dye.

Dye loading on photoanodes surface was quantitatively determined by UV/Vis spectrophotometry after calibration using diluted 0.1M NaOH aqueous solutions of N719 dye. Adsorbed dye was completely removed from oxide surface by washing with a 0.1M NaOH aqueous solution.[30] Optical absorption spectra were collected at room temperature on a PG Instruments T80 spectrophotometer (1 cm quartz cuvettes were used for liquid samples).

Diffuse reflectance FTIR spectra were collected under vacuum on a Bruker VERTEX70v spectrometer (accumulating 32 scans at a resolution of 2 cm^{-1}) and displayed in the Kubelka–Munk unit.[35] A few milligrams of each sample were mixed with KBr and loaded in the accessory for diffuse reflectance (Harrick Scientific); KBr was used as a background.

Cell fabrication was carried out using the I_3^-/I^- redox couple. The active area of the cells was 25 mm^2. Platinized FTO (5 nm thick sputtered Pt film) was used as the counterelectrode. The redox electrolyte contained 0.1M LiI, 0.05M I_2, 0.6M 1,2-dimethyl-3-n-propylimidazolium iodide, and 0.5M 4-*tert*-butylpyridine dissolved in acetonitrile. All chemicals were purchased from Sigma–Aldrich and used as received. The functional properties of the cells were investigated under simulated sunlight irradiation using an ABET 2000 solar simulator at AM 1.5G (100 mW cm^{-2}). Transient open-circuit photovoltage voltage decay (measured according to Ref. [33]) was investigated to obtain information on electron lifetime.

Received: July 4, 2011
Published online: September 26, 2011

Keywords: dye-sensitized solar cells · electrochemistry · nanocrystallites · zinc oxide

[1] M. Graetzel, *Nature* **2001**, *414*, 338.
[2] B. A. Gregg, *J. Phys. Chem. B* **2003**, *107*, 4688.
[3] B. O'Regan, M. Graetzel, *Nature* **1991**, *353*, 737.
[4] K. Keis, E. Magnusson, H. Lindstrom, S. E. Lindquist, A. Hagfeldt, *Sol. Energy Mater. Sol. Cells* **2002**, *73*, 51.
[5] T. Stergiopoulos, I. M. Arabatzis, H. Cachet, P. Falaras, *J. Photochem. Photobiol. A* **2003**, *155*, 163.
[6] P. Guo, M. A. Aegerter, *Thin Solid Films* **1999**, *351*, 290.
[7] M. K. Nazeeruddin, F. De Angelis, S. Fantacci, A. Selloni, G. Viscardi, P. Liska, S. Ito, B. Takeru, M. Graetzel, *J. Am. Chem. Soc.* **2005**, *127*, 16835.
[8] M. K. Nazeeruddin, P. Péchy, M. Graetzel, *Chem. Commun.* **1997**, 1705.
[9] Y. Cao, Y. Bai, Q. Yu, Y. Cheng, S. Liu, D. Shi, F. Gao, P. Wang, *J. Phys. Chem. C* **2009**, *113*, 6290.
[10] A. Ranga Rao, V Dutta, *Nanotechnology* **2008**, *19*, 445712.
[11] M. Law, L. E. Greene, J. C. Johnson, R. Saykally, P. D. Yang, *Nat. Mater.* **2005**, *4*, 455.
[12] J. B. Baxter, E. S. Aydil, *Appl. Phys. Lett.* **2005**, *86*, 053114.
[13] A. Vomiero, I. Concina, M. M. Natile, E. Comini, G. Faglia, M. Ferroni, I. Kholmanov, G. Sberveglieri, *Appl. Phys. Lett.* **2009**, *95*, 193104.
[14] S. Yodyingyong, Q. Zhang, K. Park, C. S. Dandeneau, X. Zhou, D. Triampo, G. Cao, *Appl. Phys. Lett.* **2010**, *96*, 073115.
[15] S. H. Ko, D. Lee, H. W. Kang, K. H. Nam, J. Y. Yeo, S. J. Hong, C. P. Grigoropoulos, H. J. Sung, *Nano Lett.* **2011**, *11*, 666.
[16] Q. Zhang, T. P. Chou, B. Russo, S. A. Jenekhe, G. Cao, *Angew. Chem.* **2008**, *120*, 2436; *Angew. Chem. Int. Ed.* **2008**, *47*, 2402.
[17] Q. F. Zhang, G. Z. Cao, *J. Mater. Chem.* **2011**, *21*, 6769.
[18] H.-M. Cheng, W.-F. Hsieh, *Energy Environ. Sci.* **2010**, *3*, 442.
[19] a) S. Haller, Servane, T. Suguira, D. Lincot, T. Yoshida, *Phys. Status Solidi A* **2010**, *207*, 2252; b) K. Nonomura, D. Komatsu, T. Yoshida, H. Minoura, D. Schlettwein, *Phys. Chem. Chem. Phys.* **2007**, *9*, 1843.
[20] M. Saito, S. Fujihara, *Energy Environ. Sci.* **2008**, *1*, 280.
[21] a) L. Kavan, M. Graetzel, *Electrochim. Acta* **1995**, *40*, 643; b) P. J. Cameron, L. M. Peter, *J. Phys. Chem. B* **2003**, *107*, 14394.
[22] N. Memarian, S. M. Rozati, E. Elamurugu, E. Fortunato, *Phys. Status Solidi C* **2010**, *7*, 2277.
[23] H. C. van de Hulst, *Light Scattering by Small Particles*, Wiley, New York, **1957**.
[24] P. E. Wolf, G. Maret, *Phys. Rev. Lett.* **1985**, *55*, 2696.
[25] P. Barthelemy, J. Bertolotti, D. S. Wiersma, *Nature* **2008**, *453*, 495.
[26] Q. F. Zhang, T. P. Chou, B. Russo, S. A. Jenekhe, G. Cao, *Adv. Funct. Mater.* **2008**, *18*, 1654.
[27] K. Keis, C. Bauer, G. Boschloo, A. Hagfeldt, K. Westermark, H. Rensmo, H. Siegbahn, *J. Photochem. Photobiol. A* **2002**, *148*, 57.
[28] T. P. Chou, Q. F. Zhang, B. Russo, G. E. Fryxell, G. Cao, *J. Phys. Chem. C* **2007**, *111*, 6296.
[29] K. Keis, J. Lindgren, S.-E. Lindquist, A, Hagfeldt, *Langmuir* **2000**, *16*, 4688.
[30] V. Thavasi, V. Renugopalakrishnan, R. Jose, S. Ramakrishna, *Mater. Sci. Eng. R* **2009**, *63*, 81.
[31] F. Sauvage, J.-D. Decoppet, M. Zhang, S. M. Zakeeruddin, P. Comte, M. Nazeeruddin, P. Wang, M. Graetzel, *J. Am. Chem. Soc.* **2011**, *133*, 9304.
[32] G. B. Deacon, R. J. Phillips, *Coord. Chem. Rev.* **1980**, *33*, 227.
[33] a) J. Bisquert, F. Fabregat-Santiago, I. Mora-Sero, G. Garcia-Belmonte, S. Giménez, *J. Phys. Chem. C* **2009**, *113*, 17278; b) A. Zaban, M. Greenshtein, J. Bisquert, *ChemPhysChem* **2003**, *4*, 859.
[34] a) P. J. Cameron, L. M. Peter, S. Hore, *J. Phys. Chem. B* **2005**, *109*, 930; b) P. J. Cameron, L. M. Peter, *J. Phys. Chem. B* **2005**, *109*, 7392; c) S. Ito, P. Liska, P. Comte, R. Charvet, P. Péchy, U. Bach, L. Schmidt-Mende, S. M. Zakeeruddin, A. Kay, M. K. Nazeeruddin, M. Graetzel, *Chem. Commun.* **2005**, 4351; d) L. M. Peter, *J. Phys. Chem. C* **2007**, *111*, 6601.
[35] a) P. Kubelka, F. Munk, *Z. Tech. Phys.* **1931**, *12*, 593; b) G. Kortüm, *Reflectance Spectroscopy*, Springer, New York, **1969**.

